ACS APPLIED ENERGY MATERIALS

Article

Tracking Compression Changes in an Aqueous Electrolyte for Real-Time H2 and O2 Gas Evolution Quantification during Total Water Splitting using BARDS.

Aaron Kang, Alanood Alkhraije, Sean McSweeney, Anas Alfarsi, Rizwan Ahmed, Jacob Krüse, Colm O'Dwyer, and Dara Fitzpatrick

ACS Appl. Energy Mater., **Just Accepted Manuscript** • DOI: 10.1021/acsaem.9b02436 • Publication Date (Web): 17 Jan 2020

Tracking Compression Changes in an Aqueous Electrolyte for Real-Time H_2 and O_2 Gas Evolution Quantification during Total Water Splitting using BARDS

Aaron Kang[1], Alanood Alkhraije[1], Seán McSweeney[2], Anas Alfarsi[1,3], Rizwan Ahmed[1,3], Jacob Krüse[4], Colm O'Dwyer[1,5,6,7], Dara Fitzpatrick*[1,3,6]

[1] School of Chemistry, University College Cork, Cork T12 YN60, Ireland

[2] BARDS Acoustic Science Labs, Cork, T12 YN60 Ireland

[3] Analytical and Biological Chemistry Research Facility (ABCRF), University College Cork (UCC), Cork, T12 YN60 Ireland.

[4] Kinetox, Kruiskruidlaan 11, 9413 BB, Beilen, The Netherlands

[5] Tyndall National Institute, Lee Maltings, Cork T12 R5CP, Ireland

[6] Environmental Research Institute, Lee Road, Cork T23 XE10, Ireland

[7] AMBER@CRANN, Trinity College Dublin, Dublin 2, D02 PD91 Ireland

*d.fitzpatrick@ucc.ie

Keywords:

Electrochemistry, Water Splitting, HER, OER, BARDS, Gas measurements, Electrode Efficiency.

Abstract

Hydrogen fuel cell technology has the potential for integration with renewable energy sources to produce electricity without the need for fossil fuels. Efforts are being made in producing cheap and effective electrodes from new materials to make hydrogen production more efficient. Gas evolution, in all cases, requires an accurate analysis of electrochemical behaviour of electrodes to quantify efficiency, improvement or stability. Knowing the exact gas volume by any method in real-time during electrochemical water splitting is urgently needed. Taking inspiration from the existing Broadband Acoustic Resonance Dissolution Spectroscopy technique, we demonstrate an original approach to continuously track the electrochemical water splitting via the gas volume evolution from hydrogen evolution reactions (HER) and oxygen evolution reactions (OER) processes. The technique may be used to unravel the true features of new electrode materials that evolve hydrogen, and correlate material electrochemistry to the true gas volume evolved in real-time.

Introduction

As the world population increases so too does the global demand for energy. The global population is projected to rise to 9.1 billion by the year 2050(1), and the world's energy consumption is expected to rise by 28% by 2040.(2) The majority of the current world's energy requirements are being fulfilled by fossil fuels, with petroleum and other liquid fuels being the largest source of energy with a market of 33% in 2015.(2) The major issue with the use of fossil fuels for energy is the combustion of hydrocarbons and their contribution to greenhouse gas emissions. There is currently a global effort to respond to the threat of climate change, signified by the signing of the Paris Agreement in 2015(3) to limit the rise of global temperatures to less than 2°C.

The use of hydrogen as a fuel source has a significant potential to be used alongside other renewable energy resources as a way to reduce the global carbon footprint. Hydrogen can be produced through non-renewable or renewable sources. Currently, the primary method of producing hydrogen is by the steam reforming of methane gas, accounting for 48% of the world's hydrogen production.(4) Hydrogen fuel cell technology is able to directly convert the chemical energy of the hydrogen fuel to electrical energy.(5-8) The International Energy Agency reported that the transport sector is responsible for 24% of the world's CO_2 emissions.(9) The use of fuel cells to replace a conventional combustion engine in vehicles would significantly help in the reduction of global greenhouse gas emissions, and fuel cell technology options are gaining traction with some automotive manufacturers.

Hydrogen fuel required for fuel cells can be produced through electrolysis and one potential source is from sun-light driven or electro-catalysed hydrogen evolution reactions from water splitting.(10-13) A limitation to scalable and ubiquitous systems for H_2 production for fuel cells is the requirement for expensive inert metals such as platinum. Efforts are being made in producing cheap, efficient electrodes from new materials that mitigate the need for costly metals (14-18), but that are also electrochemically stable at high current density, and efficiently enable HER and/or OER reactions for long periods at low over-potentials.(19) Another

drawback is the direct comparison of the efficiencies of complex electrode materials (composition, morphology etc.) with definitive platinum electrodes, obtaining a consensus on the reporting efficiencies, Tafel slopes, kinetic models and the overall nature of (bi)functional catalysis has been recommended.(20, 21) One critically important aspect remains – the ability to obtain operando quantitative measurement of the actual gas evolution during HER and OER inside the cell and inside the electrolyte itself, as opposed to extrapolation from the current, kinetics and the over-potential and other parameters, free-space pressure changes in a closed electrochemical cell, or sniffing-based detection of escaped gas.

Accurately determining either HER or OER gas volume evolution in real-time, that accounts for gas solubility and capturable volume is lacking. In spite of the explosion in recent advances in non-noble metal nanomaterials that indicated excellent, stable HER and OER capability (22-26), the direct gas volume is not examined but estimated by parameters that describe the materials electrochemical behaviour in aqueous (acidic or basic) electrolyte. Many factors affect gas evolution, for example, nano-bubble formation, concentration of OH^- or H^+ species in alkaline or acidic electrolytes, and the basic Volmer-to-Tafel mechanism of H_2 formation. A quantitative operando method of precise measuring of H_2 or O_2 volumes in total water splitting, that is determined by examining the effect of gas volume, solubility and compressibility in the *entire* electrolyte, could provide a new state-of-the-art advancement for this important renewable energy technology fuel source. Gas sniffing, direct sampling and other methods including gas chromatography (27-32) require carrier gases that measure evolved gas outside of the solution, and fail to account for solubility, the effect of the nanomaterial structure or surface chemistry on gas bubble size, trapping, and other parameters that affect the kinetics of gas evolution.

BARDS analysis is the first operando, continuous and quantitative measurement tool to track H_2 and O_2 gas volume evolution during total water splitting by monitoring the changes in the acoustic resonance within the solution caused by changes to its compressibility. The method uses BARDS to assess compressibity changes from H_2 and O_2 evolution in the form of an operando frequency change that produces a unique spectrum, which correlates to the

current (rate), solution concentration, and overall gas volume production. The method is a platform for assessing dissolved gases, and liberated gases in electrochemical reactions of which water splitting is of immediate importance and relevance, but it can be adapted to any system that displays a compressibility change to a solvent. In this case, the direct measurement of gas evolution can be correlated to the basis of a Standard Hydrogen Electrode. This offers a way of quantitiatively comparing true gas volume evolution from the myriad of new nanomaterials to an ideal Sstandard Hydrogen Electrode (SHE). This approach can mitigate against inaccuracy from interpretation of electrochemical data, when the gas volume production is the most important output from the water splitting technique. Measuring pressure changes requires a closed system which can be disadvantageous, also a very sensitive pressure sensor is required. However, BARDS allows for extrapolation of the real time volume of gas evolved at any point in time without cumulative measurement being necessary or a closed system.

The Basics of a BARDS Response

An increase in the compressibility of a solvent results in a decrease of the velocity of sound in that solvent. The velocity of sound in a liquid or gas can be obtained by $v = (K.\rho)^{-1/2}$, here *v* is the velocity of sound, ρ is the mass density and K is the compressibility defined (33) by Equation 1.

$$K = \frac{dV}{dp} \cdot \frac{1}{V} \qquad \text{Equation 1}$$

The production of small gas bubbles in a solvent has a negligible effect on the density while having a significant effect on the compressibility. The relationship between the velocity of sound and the fractional volume occupied by air bubbles was derived by Frank S. Crawford.(34) This is known as the Crawford equation, given by Equation 2.

$$\frac{v_w}{v} = \left(1 + f_a \frac{K_a}{K_w}\right)^{1/2} \qquad \text{Equation 2}$$

Where v_w and v are the velocities of sound in pure and bubble-filled water respectively, and f_a is the fractional volume occupied by gas bubbles. The compressibility ratio is defined by Equation 3.

$$\frac{K_a}{K_w} = \frac{v_w^2 \rho_w}{\gamma p} \qquad \text{Equation 3}$$

K_a is the adiabatic compressibility of dry air, K_w is the compressibility of water, ρ_w is the water density, γ is the ratio of specific heats for dry air, and p is the atmospheric pressure. In this case, $\frac{K_a}{K_w} = 1.49 \times 10^4$. The value γ is 1.40 for dry air. The corresponding values for Hydrogen (1.405) and Oxygen (1.395) are almost identical therefore the ratios are essentially fixed. For a defined liquid volume of fixed height, Equation 2 becomes Equation 4:

$$f = \frac{f_w}{\left(1 + f_a \frac{K_a}{K_w}\right)^{1/2}} \qquad \text{Equation 4}$$

where f_w is the resonance frequency of the fundamental resonance mode in pure water (also indicated as volume line, because it depends on the liquid level height and f is the resonance frequency in bubble-filled water. The minimum frequency of the BARDS response is the point where the rate of formation of gas in solution is equal to the rate of gas liberation from the surface of the solvent. The solution is at its most compressible at this point. Equation 4 can also be expressed as Equation 5;

$$f = \frac{f_w}{\sqrt{1 + 1.49x10^4 \cdot f_a}} \qquad \text{Equation 5}$$

A detailed and comprehensive outline on the principles and processes involved in BARDS analysis is given by Fitzpatrick *et al*. (35-38)

The formation of gas bubbles alters the detected resonance frequency. The gas bubbles in these experiments are produced from the electrolysis of the solution using platinum electrodes immersed in the solution, which is the standard hydrogen electrode and a model

system for total water splitting. A typical BARDS spectrum for the on-off cycle is shown in Figure 1. There is a 'shark-fin' repetition evident in the frequency – time course plot which is related to the compressibility of the solution as gas is evolved and subsequently exits the solution during the rest period.

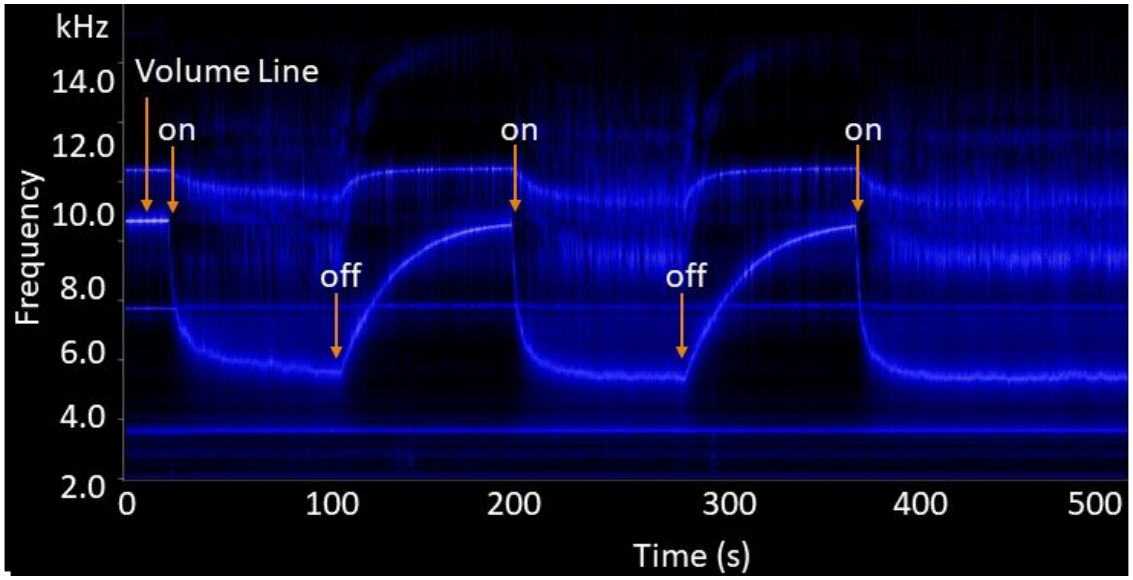

***Figure 1**: Acoustic spectra of the electrolysis of H_2SO_4 utilising Pt electrodes with applying an intermittent current. Note the overtone resonant frequency starting at 11.5 KHz which also tracks the on/off cycle.*

The BARDS spectrum obtained for the water splitting in aqueous solutions with different concentrations of H_2SO_4 under potentiostatic conditions is illustrated in Figure 2(A). These experiments were carried out in duplicate for all concentrations, and the total run time for each experiment of 700 s. Once the potential is applied, gas evolution occurs from the Pt wire surface, which affects the frequency of sound in the electrolyte. The reduction in this frequency is due to the compressibility increase from the presence of gas bubbles. The gas evolution steady-state frequency is reached after a 70 s timeframe and potential is then cut off. The minimum frequency points from the acoustic profiles of H_2 evolution during water splitting in electrolyte concentration ranging from 0.5 - 1.25 M varied from 6.8 to 5.0 kHz, respectively.

We also measured the variation of the current in parallel with the BARDS spectrum. Figure 2(B) shows the potentiostatic current response as a function of H_2SO_4 concentration. At a constant potential of 2.3 V, the magnitude of the current relates with the acoustic

frequency variation during gas evolution. Gas evolution was evaluated during total water splitting at various over-potentials in the range 2.0 – 2.5 V in the 1 M H_2SO_4 solution. A reduction in the acoustic frequency consistent with the production of gas altering the compressibility of the solution was noted at all potentials. The BARDS profiles, Figure 2(C) (and visual examination of the electrode surface) showed an increase in the rate of gas evolution and thus the total gas volume at higher over-potentials. Figure 2(D) shows the corresponding current density profile for these measurements. The average magnitude of the current density changes at a rate that is related to the frequency change and thus also the

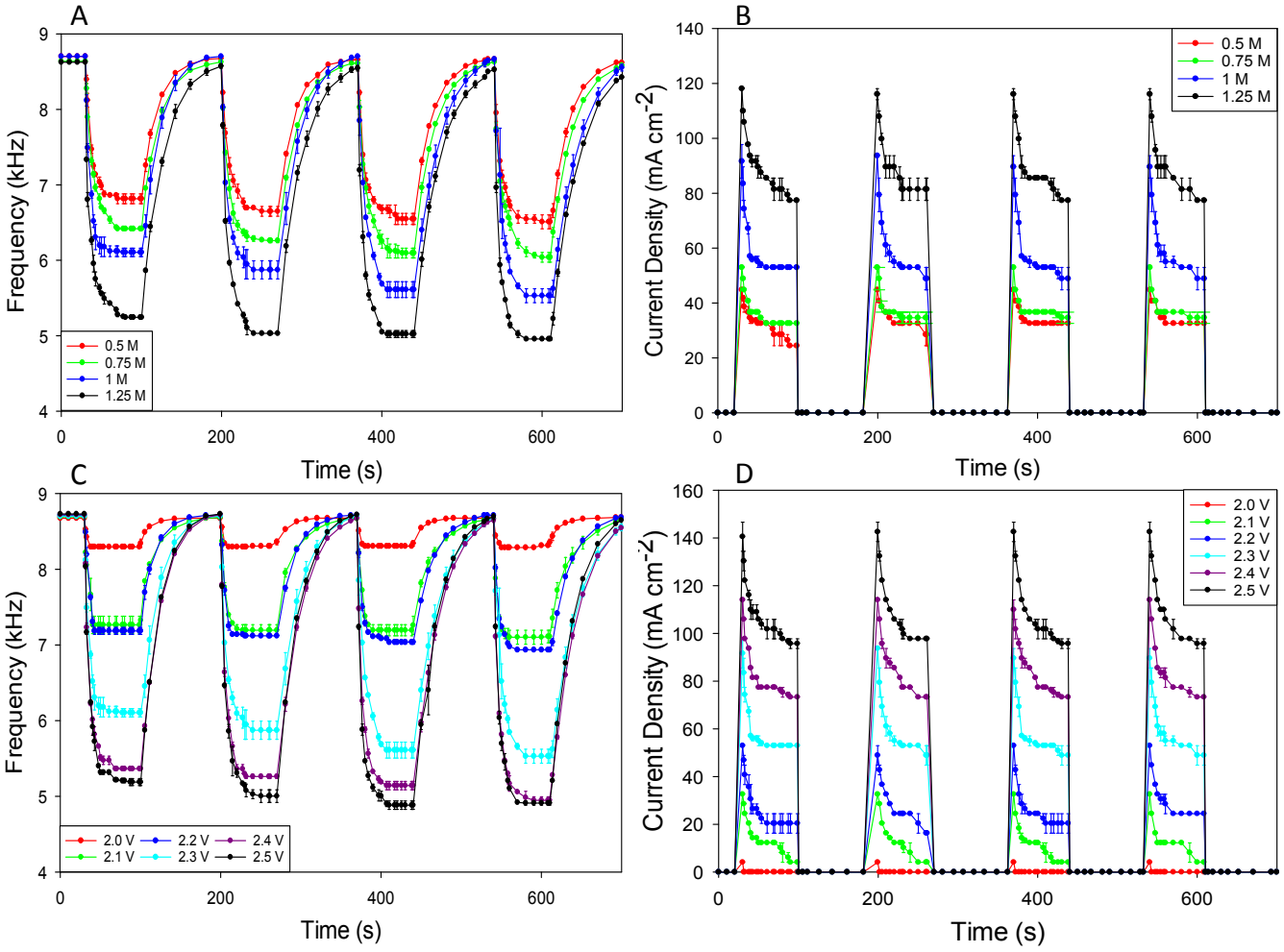

***Figure 2**: (A) BARDS spectrum showing the change in acoustic frequency measured during total water splitting at a constant potential of 2.3 V as a function of H_2SO_4 concentration in solution. Four sequential measurements are shown corresponding to 70 s durations (potential applied at 30 s, turned off at 100 s.) and a resting period of 100 s. (B) The corresponding current density measured during the BARDS spectrum acquisition of the variation of concentration. (C) BARDS spectrum of the total water splitting in a fixed concentration of 1M H_2SO_4 electrolyte at varying*

potentials in the range 2.0 – 2.5 V, and (D) the corresponding current density profiles measured over time at each of the applied potentials.

Ahmed et al., reported BARDS data to be highly reproducible and the average standard deviation across spectral data points of triplicate measurements = 0.122 kHz. This allows for a reduction in replication to duplicate measurements with an average variance of 2.06%. The variance for the data for the electrolysis experiments is 1.46 %.

The change in the measured acoustic frequency as a function of H_2SO_4 concentration were converted into a gas volume using the Crawford relation (Equation 2) to produce the spectrum illustrated in Figure 3(A). For more concentrated electrolytes, we observe an increase in gas bubble generation in solution and thus an increase in the gas volume during electrolysis. A higher maximum gas volume is attained with each successive on-off cycle for each concentration. This is possibly due to the accumulation or over-saturation of gas that has not escaped the solution once the potential is cut-off. This over-saturation contributes to the compressibility of the successive cycle.

Cells where the potential varied in the range 2.0 – 2.5 V were also examined. It is found that the acoustic frequency decreases when the current is passed through the solution which causes gas evolution and a change in the compressibility of the solvent. Higher over-potentials cause an increase in gas production and thus the total gas volume, which is observed in the frequency decrease due to changes in compressibility. This result was used to calculate the volume of gas produced using Equation 2 and is shown in Figure 3(B). The larger gas production that is observed with an increase in potential is due to the rise in the electrical current which is shown in Figure 2(D) resulting in a larger quantity of passed charge. Like the variation of concentration with periodic applied potential, the maximum gas volume increases to successively higher values in each on-off run and can be explained in a similar manner. We showed in Figure 2(D) that the increase in the potential passed through the solution of H_2SO_4 leads to an increase in the current. The resistance is initially constant in the solution and thus the increase in the potential causes a direct increase in the current. The

current observed for the potential of 2.0 V, was below the range limit of detection by the instrument, therefore was not observed.

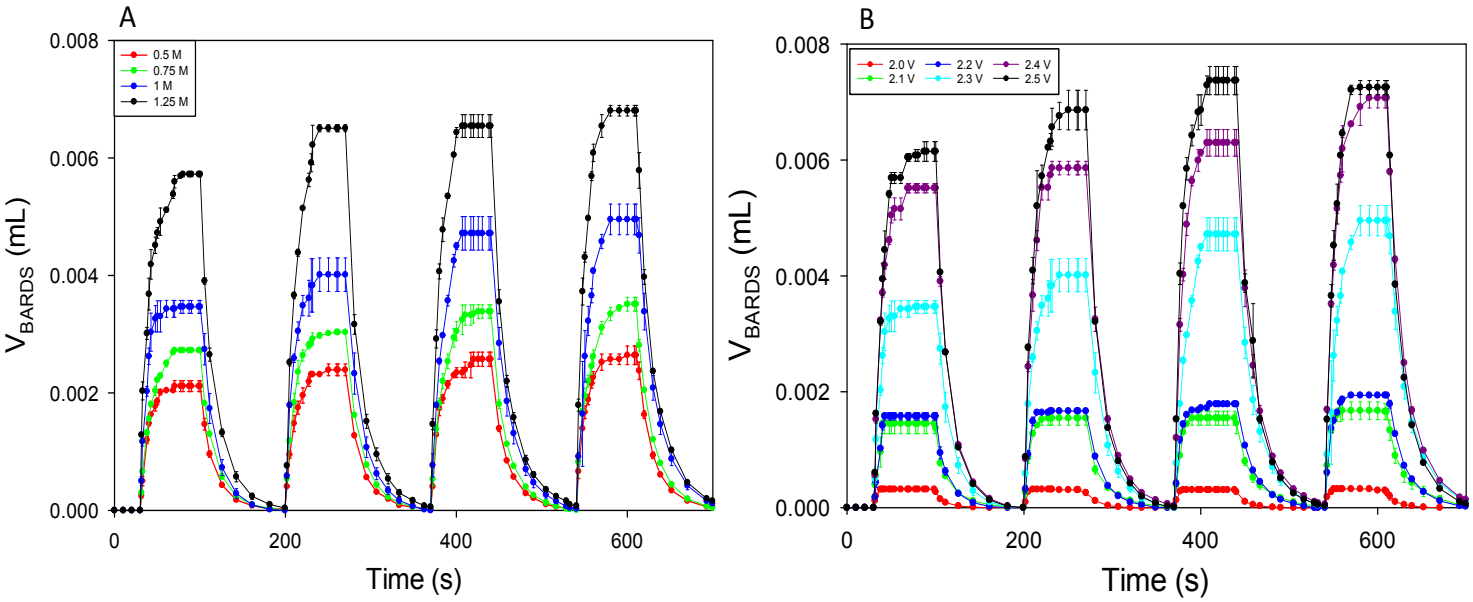

***Figure 3**: Volume-time data calculated from the BARDS spectrum, using the Crawford equation (Equation 2) for: (A) BARDS spectrum showing the change in acoustic frequency measured during total water splitting at a constant potential of 2.3 V as a function of H_2SO_4 concentration in solution. (B) BARDS spectrum of total water splitting in a 1M H_2SO_4 electrolyte at constant potentials in the range 2.0 – 2.5 V. Four sequential measurements are shown corresponding to 70 s durations and a rest period of 100 s.*

The BARDS data for gas evolution also provides insight into the remnant bubbles on the electrode surface once the potential is cut off. For electrodes that retain some surface-bound gas bubbles after the first cycle, the acoustic spectra in the successive on-off cycles specifically account for cumulative gas evolution. BARDS can quantify the relative contribution of surface-bound bubbles in successive water splitting experiments to potentially compare more complex porous materials against a standard Pt wire. A longer time is required for the fundamental curve to return to its steady state volume line by increasing electrolyte concentration once the potential is turned off. The significance of this consistent observation is that high concentration electrolytes, which evolve gas in higher volumes, require a longer time for all gas bubbles to be removed from the solution once the potential is turned off. However, there is not a simple linear relation between frequency (f_w/f) and gas volume. Reaching steady state is poorly defined, since it is assumed that gas volume disappearance proceeds according to a first order process (implying exponential return). A larger response

will require a longer time to drop below a certain threshold value that defines steady state. A more objective criterion is the elimination rate constant, k_{el}, obtained from the gas volume plot which relates directly to it. Analysis of the k_{el} values in the electrolyte concentration series does not show a consistent effect. If there had been any effect, this may be explained by an increase in electrolyte viscosity causing bubble loss to occur more slowly in more concentrated (acidic) electrolytes.

The gas evolution volume also relates with the total current density (*vide infra*) at constant over-potential and can be measured for the first time directly in the total electrolyte volume. For any concentration, the initial current density reaches a maximum and as seen previously, decreases over time until it reaches a steady minimum point, possibly due to the added resistance from the presence of gas bubbles adhering to the electrodes.(39) Once the potential is cut-off, gas elimination follows a specific, repeatable profile. For such a well-defined Pt-based cell that undergoes total water splitting at cathode and anode, H adsorption to Pt is well-known resulting in Volmer-to-Tafel steps in acidic electrolyte that generate molecular hydrogen, but becomes considerably more complex for new functional electrocatalytic material designed to maximise efficiency, rate, reduce over-potential and enhance stability at low cost. For example, the plethora of non-platinum and non-noble metal electrocatalysts differ not only in energetics, but in morphology, porosity, surface charge and defect chemistry, which affect bubble nucleation, size, trapping, adsorption and the rate of evolution. BARDS profiles could be the first direct technique to determine the onset of gas evolution at different over-potentials and determine whether certain degrees of porosity used in high surface area catalysts limit the effective rate of gas evolution compared to planar electrodes.

The value of k_{el} can be determined from the decay of the gas volume, observed after switching off the current at t = T, by transforming the gas volume (V_{BARDS}) for t > T to ln (V_{BARDS}). This can also be done if the volume at steady state (V_{ss}) has not yet been reached before switching off the voltage. The gas volumes and associated current densities from the electrolysis of 1M H_2SO_4 solution at 2.3 V for each on/off cycle, shown in Figure 4(A) and (B),

was used in this analysis. We note an increasing maximum gas volume in succeeding cycles in Figure 4 (A), which is likely due to accumulative over-saturation of gas, which has not escaped the solution and thus contributes to the change in compressibility of the subsequent

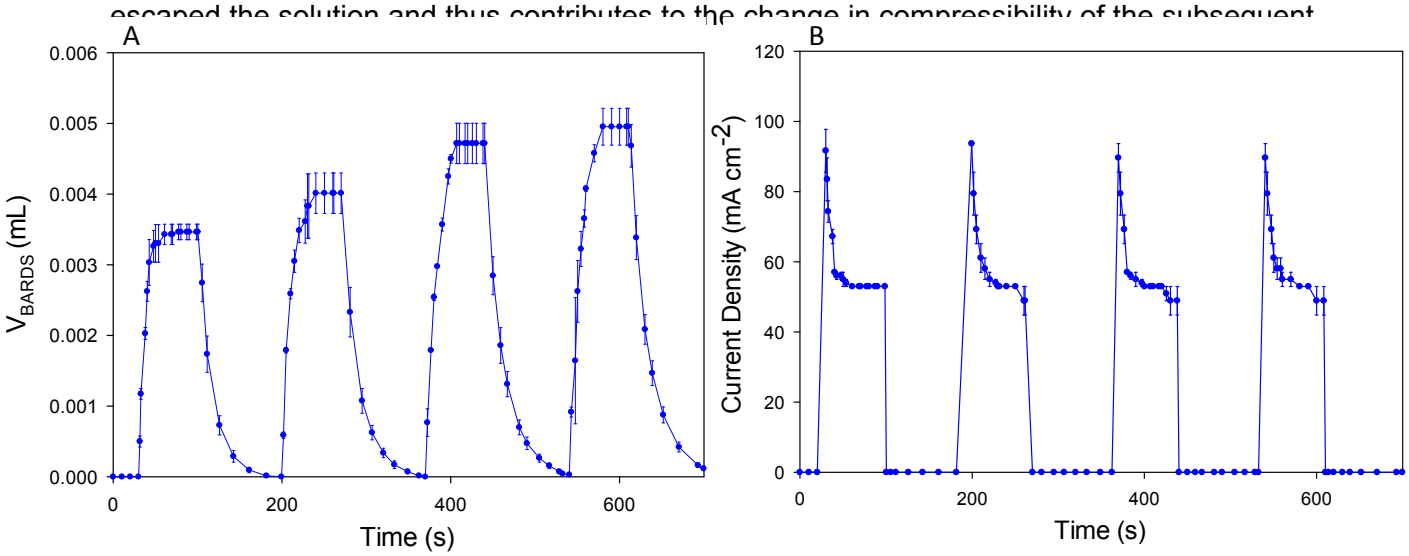

***Figure 4**: (A) Volume-time data calculated, using the Crawford equation (Equation 2), from the BARDS spectrum for gas evolution during water splitting at a constant potential of 2.3 V in an aqueous 1 M H_2SO_4 solution for four successive on/off cycles. (B) Corresponding current density measured during BARDS analysis acquired at a potential of 2.3 V in each successive cycle.*

The theoretical volume of gas produced during the electrolysis reaction and the actual observed volume of gas was calculated from the process detailed in Supporting Information Calculations S1. We computed a quantitative comparison using gas volume changes in time derived from the BARDS frequency data, and the theoretical volume of gas produced by electrolysis. The calculations of the total gas volume produced by BARDS (V_B), and also the theoretical volume by the Faraday equation (V_F) are shown in Table 1. The ratio between the observed (V_B) and expected values (V_F) varies between 0.077 and 0.087, with an average of 0.084. This is approximately a 12× lower than theoretically predicted, assuming a single electron electrochemical process for hydrogen with complete Faradaic efficiency. If the bare electrodes are placed too close to the liquid surface, it is likely that some of the gas bubbles

will not enter the bulk solution and escape immediately. This will thus reduce the BARDS response.

Table 1: Comparison of the observed total volume of gas produced (V_B) and theoretical total volume of gas produced (V_F) for the water splitting at a Pt electrode in variation in 1 M H_2SO_4 solution at an applied voltage of 2.3 V for 4 successive cycles.

	V_t (mL s)	k_{el} (s^{-1})	V_B (mL)	Q_t (C cm^{-2})	V_F (mL)	$\frac{V_B}{V_F}$
1st Cycle	0.278036	0.059408	0.016518	4.371636456	0.200337156	0.082449
2nd Cycle	0.321934	0.050218	0.016167	4.577141141	0.209754733	0.077074
3rd Cycle	0.373648	0.045361	0.016949	4.196381874	0.192305837	0.088136
4th Cycle	0.405402	0.041899	0.016986	4.240023218	0.194305771	0.087418
Average	0.344755		0.016655	4.346295672		0.083769

The value of k_{el} is determined from the first order return of the gas volume to zero and in Figure 5 we show the gas volume data (Figure 4(A)) from which k_{el} is determined for each cycle of the electrolysis of 1 M H_2SO_4 solution at a potential of 2.3 V. Identical volume-time graphs for each potential and concentration examined are also provided in Supporting Information Figure S1-8.

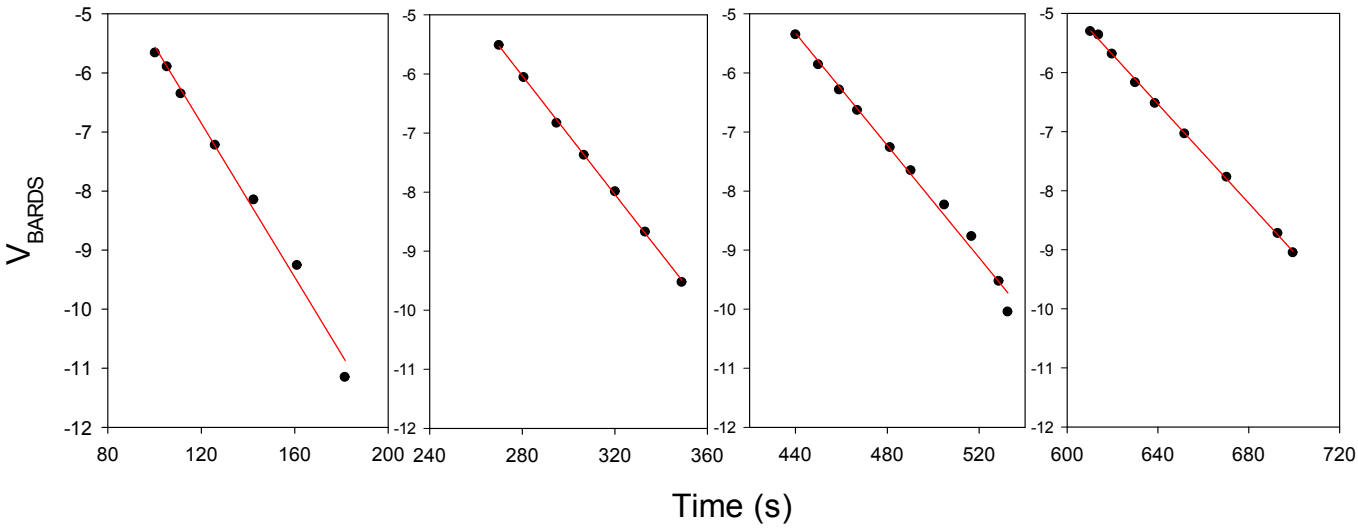

***Figure 5**: The variation of ln(V_{BARDS}) with time observed in an aqueous 1 M H_2SO_4 solution after the voltage (2.3 V) is turned off for each of the four successive on/off cycles (left to right = cycles 1 – 4) used to determine k_{el}. The slope equates to -k_{el}.*

During quantitative analysis of BARDS for gas volume measurement during water splitting, we observe variations in the parameters that define the total gas volume V_B, namely V_t and k_{el}. The product of V_t and k_{el} (i.e. V_B) does show much less variation, implying an elimination rate compensation of the change in integrated BARDS response in each cycle. We note a tendency for k_{el} to reduce in value in each successive cycle and accordingly, the return to equilibrium becomes gradually slower. We rationalise the variation in k_{el} and V_t values from BARDS, and the consistent gas volume V_B as follows. After switching off the current we assume some remnant dissolved H_2 and O_2 in the solution, so a gas oversaturation. Individual gas bubbles still present in the solution may then contribute to the volume of all dissolved gas, V_t, thereby growing in volume in each successive cycle. This process will then partly counteract the decrease in gas bubble volume via liberation at the liquid surface, i.e. k_{el} reduces with cycle. In the correct calculation of the BARDS total volume (V_B), the true k_{el} real should be used, and this k_{el} is expected to be constant for cycle 1-4 in Figures 4 and 5, implying a cyclic increase in V_B allowing observation and determination of dissolved gas oversaturation.

The total gas volume measured by BARDS, V_B, and the integrated charge, Q_t, obtained from potentiostatic I-t profiles during total water splitting were also analysed as a function of applied voltage and H_2SO_4 concentration in Figure 6. The associated calculation data for Figure 6 is shown in Supporting Information Tables S2 and S3 for variation in concentration and potential respectively. It represents a graphic summary of the analysis of all experimental data obtained in this study. All the data used in the plots in Figure 6 were averaged values of the 4 cycles in each of the experiments.

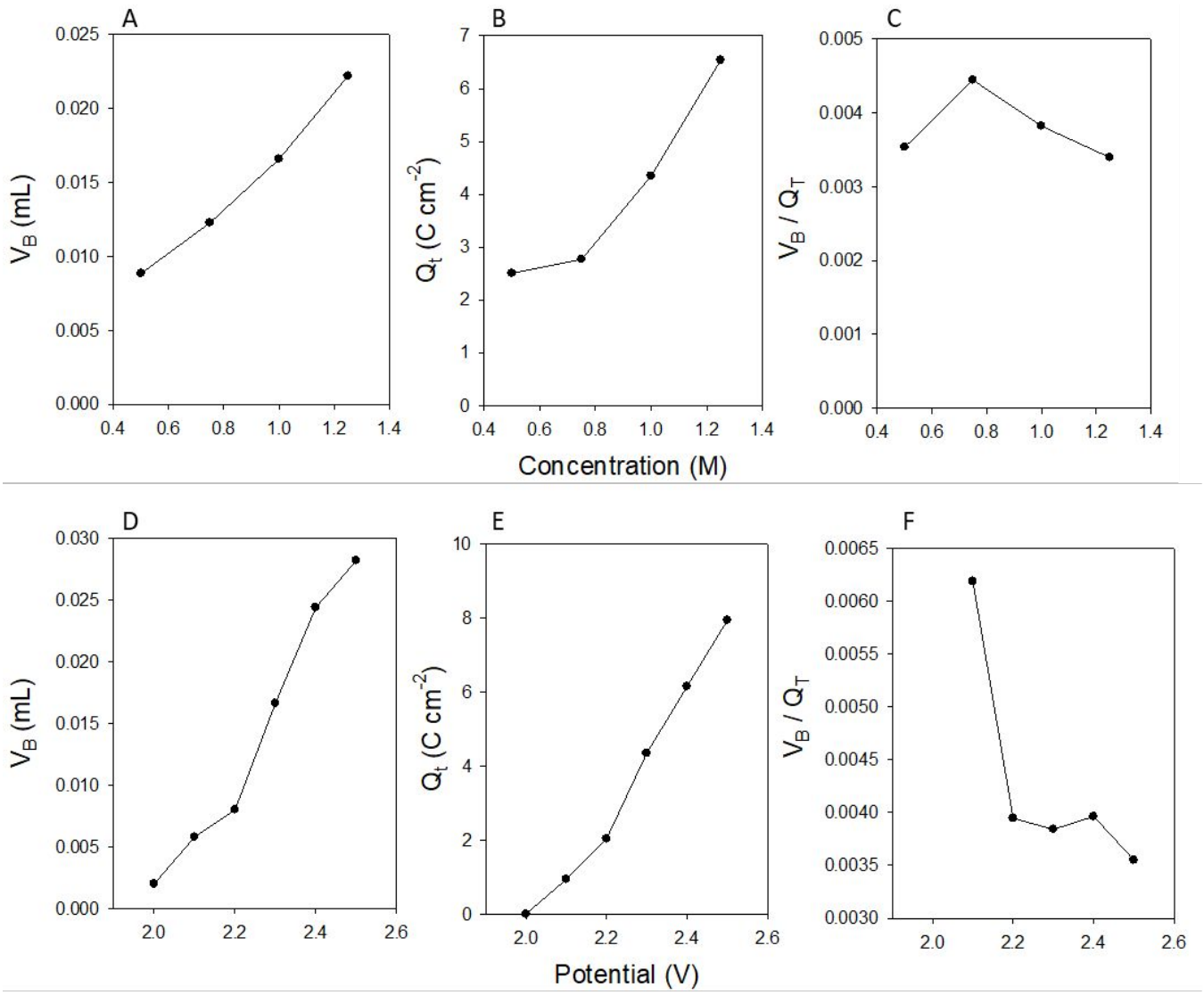

***Figure 6**: (A) Gas volume calculated from BARDS spectra, V_B and (B) corresponding integrated total charge Q_t as a function the H_2SO_4 concentration examined at a constant potential of 2.3 V. (C) The relationship between the V_B and Q_t as a function of the H_2SO_4 concentration examined at a constant potential of 2.3 V. (D) The variation of V_B and (E) total charge Q_t as a function of applied voltage tested at a constant concentration of 1M of H_2SO_4. (F) The relationship between the V_B and Q_t as a function of applied voltage tested at a constant concentration of 1M of H_2SO_4. The averaged values of the 4 cycles were used.*

For the concentration series, Figure 6 (A) – (C), the V_B to Q_t ratio is relatively constant over the whole concentration range that was tested. Figure 6 (C) shows an almost linear

relationship. The potential series, Figure 6 (D) – (F), also shows that the V_B is more or less linearly related to Q_t in the range of 2.2 – 2.5 V. The data point at 2.0 V was not included in Figure 6 (F) since the Q_t observed was zero. The data point at 2.1 V as an outlier to the trend seen in the range of 2.2 – 2.5 V.

BARDS Analysis of HER and OER in Half Cells

There is currently challenges in achieving faradaic correlation between the full cell total water splitting electrolysis and the corresponding half-cell electrolysis reactions. Figure 7 demonstrates the BARDS spectrum comparison of the full cell electrolysis reaction, at a potential of 2.3 V and a concentration of 1 M H_2SO_4, with the two half-cell electrolysis reactions, at a potential of 4.0V and concentration of 1 M H_2SO_4.

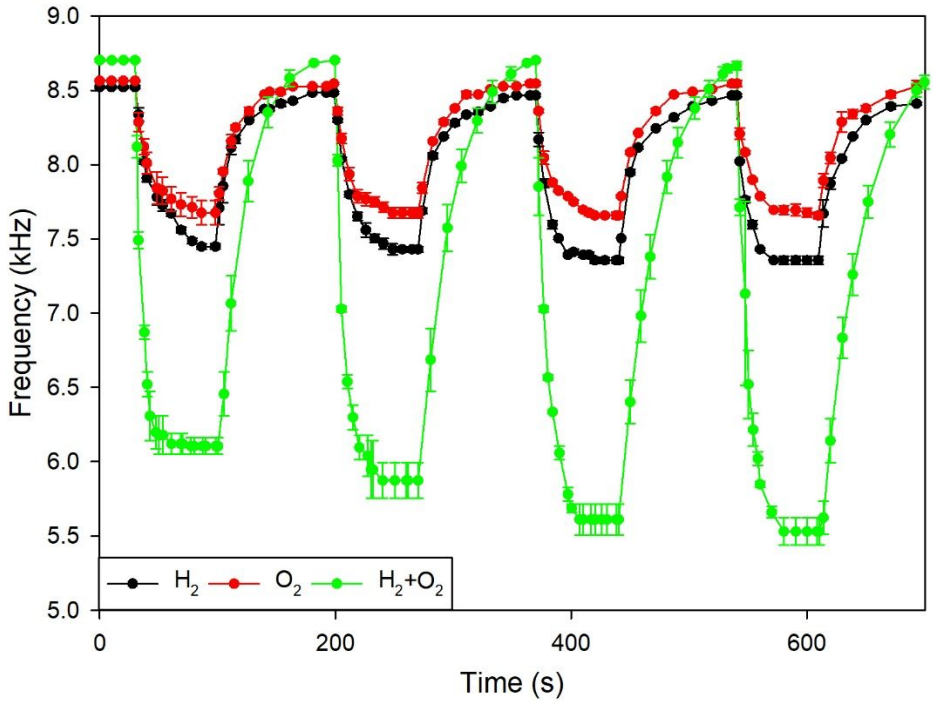

***Figure 7**: BARDS spectrum for gas evolution during full cell water splitting at a constant potential of 2.3 V in an aqueous 1 M H_2SO_4 solution for four successive on/off cycles and the two half-cell water splitting at a constant potential of 4.0 V in an aqueous 1 M H_2SO_4 solution for four successive on/off cycles.*

Figure 8 (A) illustrates the BARDS spectrum obtained for the total water splitting reaction at the Pt surface in H_2SO_4 under constant potential of 4.0 V and concentration of 1 M H_2SO_4, showing both full cell and half-cell reactions. The full cell reaction and the two half-cell

reactions were observed and measured independently. Figure 8 (B) shows the gas volumes calculated using the Crawford equation (Equation 2). This further demonstrated the discrepancy between the full cell reaction and the two half-cell reactions.

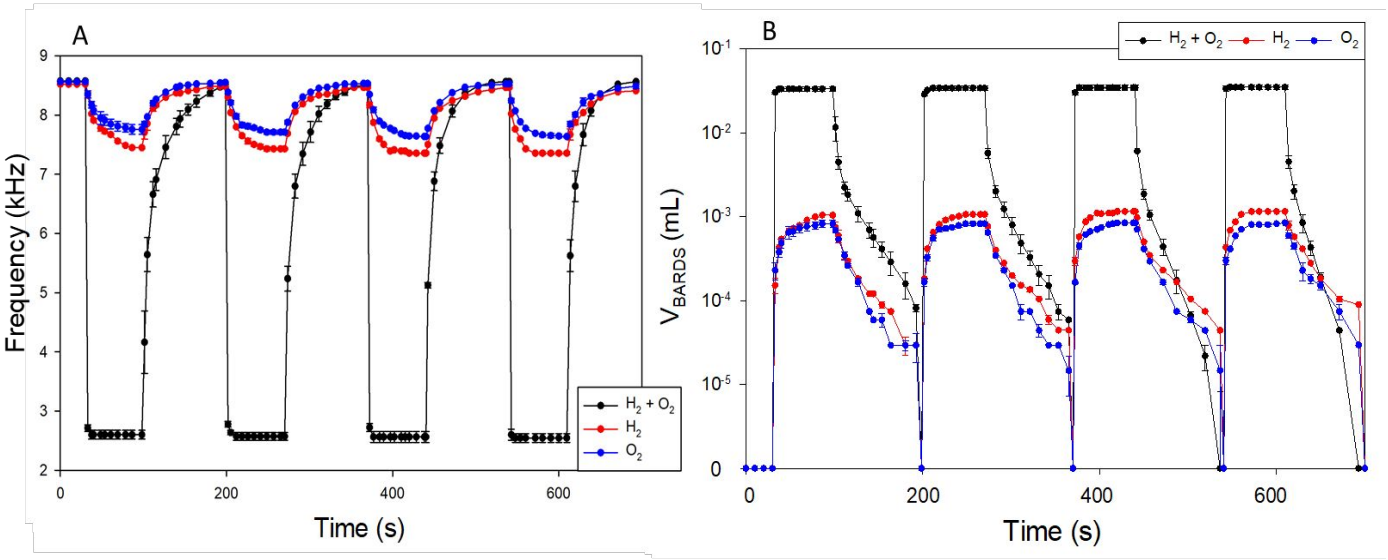

Figure 8: *(A) BARDS spectrum for gas evolution during full cell water splitting at a constant potential of 4.0 V in an aqueous 1 M H_2SO_4 solution for four successive on/off cycles and the two half-cell water splitting at a constant potential of 4.0 V in an aqueous 1 M H_2SO_4 solution for four successive on/off cycles. (B) The corresponding volume-time data calculated, using the Crawford equation (Equation 2), from the BARDS spectrum for gas evolution.*

Based on simple stoichiometric factors there should be a 2:1 ratio in gas volume of H_2:O_2. This is evidently not the case in the half-cell experiments. A major factor in the difference between measurements and expectations is due to the difference in current density passed through both systems. This is illustrated by the corresponding current density data obtained in parallel to the BARDS spectra, Figure 9.

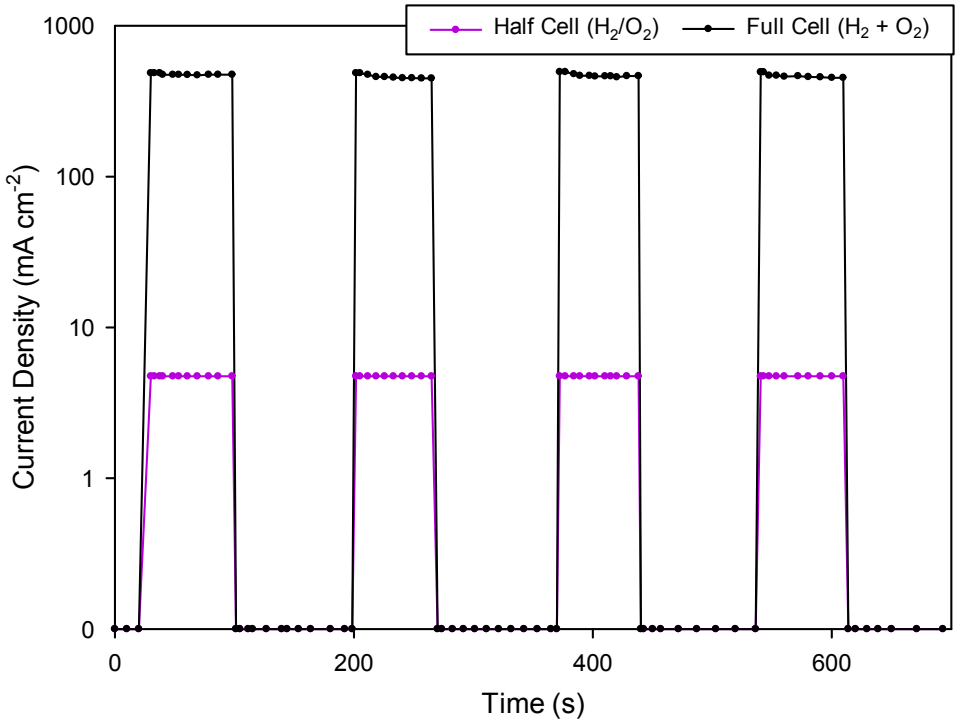

***Figure 9**: The corresponding current density measured during the BARDS analysis of full cell water splitting at a constant potential of 4.0 V in an aqueous 1 M H_2SO_4 solution for four successive on/off cycles and the two half-cell water splitting at a constant potential of 4.0 V in an aqueous 1 M H_2SO_4 solution for four successive on/off cycles.*

The half-cell reactions require an altered setup with a greater distance between the electrodes with half-cells separated by a salt bridge. This salt bridge in turn contributes to a larger total resistance in the system. Since each gas requires measurement in a single container so that the acoustic frequency is fundamentally linked to compressibility changes, a full cell setup requires an electrochemical cell with two separate beakers, essentially. This increase in resistance impedes current flow, resulting in a current density that is lower by two orders of magnitude. The increased resistance can almost entirely be ascribed to the salt bridge in the double half-cell setup, but BARDS spectra can be accurately acquired once HER and OER processes occur in each cell Alternative salt bridge or ionically conductive membranes may be considered in future developments, but these modification are not trivial since the acoustic resonance fo the electrochemical cell should remain unchanged for each half cell.

Conclusions

We have demonstrated that Broadband Acoustic Resonance Dissolution Spectroscopy is capable of real-time tracking and quantification of the gas evolution in water splitting directly within the electrolyte in full or half-cells. This is the first operando measurement that tracks changes in the compressibility of a solvent, in this case the hydrogen and oxygen evolution processes during electrolysis of an aqueous acidic solution at a Pt surface, i.e.. The sensitivity and reproducibility of BARDS provides unique acoustic spectra for gas evolution during HER and OER due to the production of gas bubbles at the platinum electrode surfaces. The approaches provides quantitative measurements of total gas evolution volumes at a Pt surface at a series of higher over-potentials, and in different acidic concentration (pH), linking the current density to the actual gas production and liberation rate from directly within the electrode and electrolyte. Being able to quantify gas evolution, including measurement of dissolved gases and liberated gas volumes during water splitting can be adapted to develop new knowledge on the nature of gas bubble formation, gas evolution rate and the factors that influence the efficiency of water splitting using complex morphologies of non-noble metal electro or photocatalysts for H_2 production, and uniquely accounts for both liberated and dissolved gases that are a result of the total charge. The BARDS technique could be employed to characterise the efficiency and quality of newly produced electrodes in a low cost and rapid way to contribute in the attempts to reduce the cost of hydrogen production and promote greener energy production.

Experimental

Materials

The following materials were purchased from Sigma-Aldrich and Emsure: platinum wire (STBD6506V) and sulphuric acid (K47143980540). Deionised water was used for preparation of all solutions used in the experiments.

Instrumentation

A BARDS spectrometer procured from BARDS Acoustic Science Labs Ltd. was used to investigate the BARDS response for the electrolysis reactions. It consists of a glass vessel with a microphone attached above the glass rim, a magnetic stirrer, and a follower. The glass vessel contains 50 mL of an aqueous sulphuric acid solution. A 250 mL stock solution of sulphuric acid is prepared using 98% concentrated sulphuric acid. The required amount is calculated from Supporting Information Table S1, carefully measured using a graduated cylinder and transferred to a 250 mL volumetric flask. The volume of the solution in the volumetric flask is adjusted to 250 mL with deionised water. An image of the full cell set-up is shown in Figure 10.

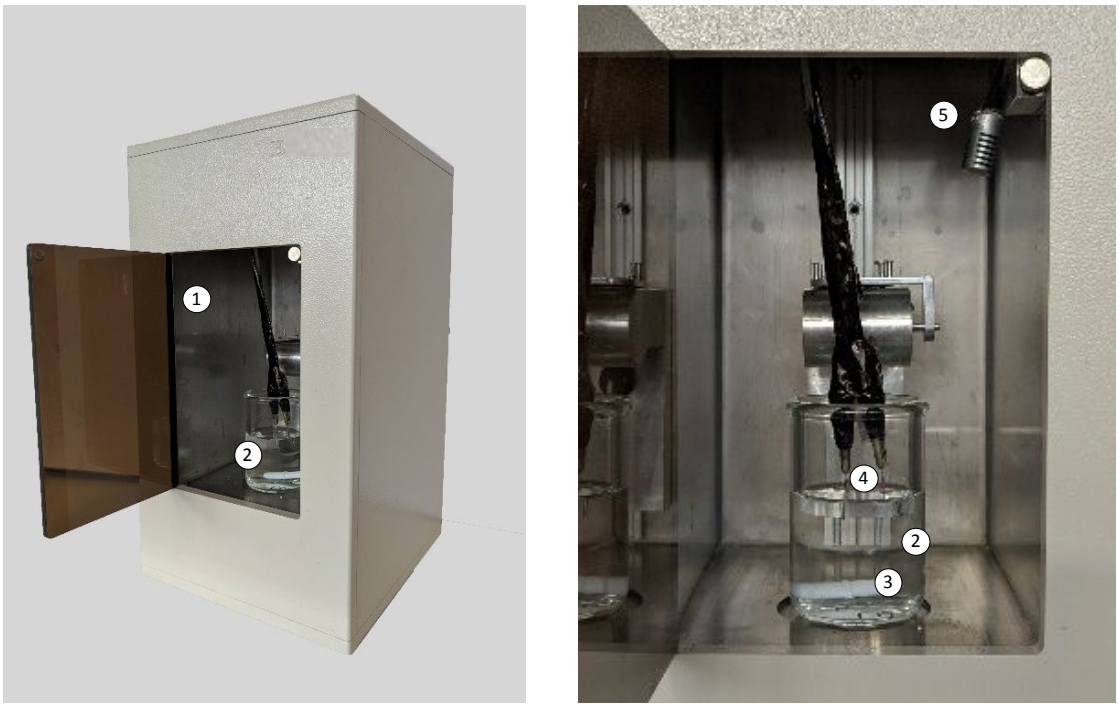

Figure 10*: Experimental set-up of the BARDS instrumentation for the analysis of SHE. 1: BARDS chamber; 2: glass vessel; 3: magnetic follower; 4: two Pt electrodes (cathode and anode); 5: microphone.*

The two electrodes are connected to a direct current power supply unit via crocodile clips and are held in place. The voltage used was ≥ 1.9 V. Although electrolysis is possible at

voltages as low as 1.23 V, the limitations of our apparatus would not allow for current flow or investigations below 1.9 V. A possible reason could be the in-line resistance of the current metre and/or the length of the wires used. The cathode and anode electrodes used are of 0.5 mm and 1 mm diameter respectively and are immersed into the solution to a depth of 0.5 cm, giving a total surface area of approximately 0.25 cm^2. The glass vessel is placed off set from the centre of the magnetic stirrer so as the follower is able to gently tap the inner walls of the glass vessel to induce an acoustic response. The acoustic resonances are captured by the microphone and converted into a spectrum using a PC. The frequency of resonances that are recorded range form 0-20 kHz. Data points from the spectrum obtained from the software are manually extracted and plotted into a graph using SigmaPlot 12.5 software.

The tracking of a single half-cell reaction of the total water splitting through electrolysis uses a modified set-up, in order to accommodate two glass vessels. Two glass vessels are used and filled with same volume (50 mL) of solution being tested. The cathode electrode is submerged in one of the glass vessels and the anode in the other. The distance between the two platinum electrodes is 27cm. The cathode electrode used is of 0.5 mm in diameter and immersed into the solution to a depth of 4 cm. The anode electrode is 1 mm in diameter respectively and are immersed into the solution to a depth of 2 cm. This gives a total surface area of approximately 0.633 cm^2 per electrode. A U-shaped salt bridge is filled with the desired saturated salt solution and used to connect both of the glass vessels. The magnetic follower is placed in the glass vessel being tested. The half-cell electrolysis reactions can be tracked independently using this setup.

Experimental Procedure

The spectrometer records the steady state resonances of the system, known as the volume line, as a reference for the first thirty seconds. The potential is applied after 30 s, passing electrical current through the solution. The electrical current is passed periodically, with a 70 s on period and a 100 s resting period. The fundamental curve is allowed to return to the

volume line before the potential is reapplied. Spectra were recorded for a total of 700 s. All experiments were performed in duplicate and an average reading with error bars is presented. The measured acoustic profiles are highly reproducible under standard conditions.

Supporting Information.

- Details of sulfuric acid electrolyte concentrations, gas elimination curves for each cycle as a function of H_2SO_4 concentration and applied voltage.
- Background theory for estimated gas volumes and associated calculations are also provided.
- Additional simulations of water oxidation processes during BARDS are provided together with details on the calculation of the k_{el} and k_{prod} parameters.
- This information is available free of charge via the internet at http://pubs.acs.org.

Funding Sources and Acknowledgements

We would like to thank the Saudi Ministry of Education for the postgraduate grants of Alanood Alkhraije and Anas Alfarsi to part fund this work. This work was part supported by Alltech Ltd. and the Irish Research Council who sponsored the support for Rizwan Ahmed's studentship under grant number IRC/EPSPG/2014/84.

Conflicts of Interest

We would like to state that Dr. Dara Fitzpatrick and Dr. Seán McSweeney are directors of BARDS Acoustic Science Labs Ltd.

References

1. Publications, U. N., World Population Prospects, Data Booklet - 2015 Revision. United Nations Publications: 2016.
2. Administration, U. S. E. I. International Energy Outlook 2017; DOE/EIA-0484(2017); 14/09/2017, 2017.
3. UNFCCC Adoption of the Paris Agreement; FCCC/CP/2015/L.9/Rev.1; 2015.
4. Santhanam, K. S.; Press, R. J.; Miri, M. J.; Bailey, A. V.; Takacs, G. A., Introduction to hydrogen technology. John Wiley & Sons: 2017.
5. Steele, B. C.; Heinzel, A., Materials for fuel-cell technologies. In Materials For Sustainable Energy: A Collection of Peer-Reviewed Research and Review Articles from Nature Publishing Group, World Scientific: 2011; pp 224-231.
6. Bashyam, R.; Zelenay, P., A class of non-precious metal composite catalysts for fuel cells. Nature 2006, 443 (7107), 63-66.
7. Schlapbach, L.; Züttel, A., Hydrogen-storage materials for mobile applications. Nature 2001, 414 (6861), 353-358.
8. Shao, Z.; Haile, S. M., A high-performance cathode for the next generation of solid-oxide fuel cells. Nature 2004, 431 (7005), 170-173.
9. IEA, CO2 Emissions from Fuel Combustion 2017. OECD Publishing: 2017.
10. Electrocatalysis for the generation and consumption of fuels. Nature Reviews Chemistry 2018, 2, 0125.
11. Voiry, D.; Shin, H. S.; Loh, K. P.; Chhowalla, M., Low-dimensional catalysts for hydrogen evolution and CO2 reduction. Nature Reviews Chemistry 2018, 2, 0105.
12. Fujishima, A.; Honda, K., Electrochemical photolysis of water at a semiconductor electrode. Nature 1972, 238 (5358), 37-8.
13. Shaner, M. R.; Atwater, H. A.; Lewis, N. S.; McFarland, E. W., A comparative technoeconomic analysis of renewable hydrogen production using solar energy. Energy & Environmental Science 2016, 9 (7), 2354-2371.
14. Gao, M.-R.; Xu, Y.-F.; Jiang, J.; Yu, S.-H., Nanostructured metal chalcogenides: synthesis, modification, and applications in energy conversion and storage devices. Chemical Society Reviews 2013, 42 (7), 2986-3017.
15. Le Goff, A.; Artero, V.; Jousselme, B.; Tran, P. D.; Guillet, N.; Métayé, R.; Fihri, A.; Palacin, S.; Fontecave, M., From hydrogenases to noble metal–free catalytic nanomaterials for H2 production and uptake. Science 2009, 326 (5958), 1384-1387.
16. Kim, T. W.; Choi, K.-S., Nanoporous BiVO4 photoanodes with dual-layer oxygen evolution catalysts for solar water splitting. Science 2014, 343 (6174), 990-994.
17. Chen, W.-F.; Wang, C.-H.; Sasaki, K.; Marinkovic, N.; Xu, W.; Muckerman, J.; Zhu, Y.; Adzic, R., Highly active and durable nanostructured molybdenum carbide electrocatalysts for hydrogen production. Energy & Environmental Science 2013, 6 (3), 943-951.
18. Luo, J.; Im, J.-H.; Mayer, M. T.; Schreier, M.; Nazeeruddin, M. K.; Park, N.-G.; Tilley, S. D.; Fan, H. J.; Grätzel, M., Water photolysis at 12.3% efficiency via perovskite photovoltaics and Earth-abundant catalysts. Science 2014, 345 (6204), 1593-1596.
19. Doyle, R. L.; Godwin, I. J.; Brandon, M. P.; Lyons, M. E., Redox and electrochemical water splitting catalytic properties of hydrated metal oxide modified electrodes. Physical Chemistry Chemical Physics 2013, 15 (33), 13737-13783.
20. Voiry, D.; Chhowalla, M.; Gogotsi, Y.; Kotov, N. A.; Li, Y.; Penner, R. M.; Schaak, R. E.; Weiss, P. S., Best Practices for Reporting Electrocatalytic Performance of Nanomaterials. ACS Nano 2018, 12 (10), 9635-9638.
21. McCrory, C. C. L.; Jung, S.; Peters, J. C.; Jaramillo, T. F., Benchmarking Heterogeneous Electrocatalysts for the Oxygen Evolution Reaction. Journal of the American Chemical Society 2013, 135 (45), 16977-16987.
22. Zheng, Y.; Jiao, Y.; Zhu, Y.; Li, L. H.; Han, Y.; Chen, Y.; Du, A.; Jaroniec, M.; Qiao, S. Z., Hydrogen evolution by a metal-free electrocatalyst. Nature communications 2014, 5, 3783.
23. Grewe, T.; Deng, X.; Weidenthaler, C.; Schüth, F.; Tüysüz, H., Design of ordered mesoporous composite materials and their electrocatalytic activities for water oxidation. Chemistry of Materials 2013, 25 (24), 4926-4935.

24. Zou, X.; Zhang, Y., Noble metal-free hydrogen evolution catalysts for water splitting. Chemical Society Reviews 2015, 44 (15), 5148-5180.
25. Yin, Q.; Tan, J. M.; Besson, C.; Geletii, Y. V.; Musaev, D. G.; Kuznetsov, A. E.; Luo, Z.; Hardcastle, K. I.; Hill, C. L., A fast soluble carbon-free molecular water oxidation catalyst based on abundant metals. Science 2010, 328 (5976), 342-345.
26. Smith, R. D.; Prévot, M. S.; Fagan, R. D.; Zhang, Z.; Sedach, P. A.; Siu, M. K. J.; Trudel, S.; Berlinguette, C. P., Photochemical route for accessing amorphous metal oxide materials for water oxidation catalysis. Science 2013, 340 (6128), 60-63.
27. Hashimoto, K.; Iwayanagi, H.; Fukushima, H., Measurement of gas evolution and absorption from materials used in vacuum tubes. Vacuum 1960, 10 (1), 92-99.
28. Hou, Y.; Abrams, B. L.; Vesborg, P. C.; Björketun, M. E.; Herbst, K.; Bech, L.; Setti, A. M.; Damsgaard, C. D.; Pedersen, T.; Hansen, O., Bioinspired molecular co-catalysts bonded to a silicon photocathode for solar hydrogen evolution. Nature materials 2011, 10 (6), 434.
29. Ai, L.; Gao, X.; Jiang, J., In situ synthesis of cobalt stabilized on macroscopic biopolymer hydrogel as economical and recyclable catalyst for hydrogen generation from sodium borohydride hydrolysis. Journal of Power Sources 2014, 257, 213-220.
30. Loghmani, M. H.; Shojaei, A. F., Hydrogen production through hydrolysis of sodium borohydride: Oleic acid stabilized Co–La–Zr–B nanoparticle as a novel catalyst. Energy 2014, 68, 152-159.
31. Laurent, C.; Scenini, F.; Monetta, T.; Bellucci, F.; Curioni, M., The contribution of hydrogen evolution processes during corrosion of aluminium and aluminium alloys investigated by potentiodynamic polarisation coupled with real-time hydrogen measurement. npj Materials Degradation 2017, 1 (1), 6.
32. Chen, M.-M.; Su, H.-F.; Xie, Y.; He, L.-F.; Lin, S.-C.; Zhang, M.-L.; Wang, C.; Xie, S.-Y.; Huang, R.-B.; Zheng, L.-S., Sniffing with mass spectrometry. Science Bulletin 2018, 63 (20), 1351-1357.
33. Wood, A. B., A textbook of sound; being an account of the physics of vibrations with special reference to recent theoretical and technical developments. The Macmillan company: New York, 1930; p xiv, 519 p.
34. Crawford, F. S., The hot chocolate effect. American Journal of Physics 1982, 50 (5), 398-404.
35. Fitzpatrick, D.; Kruse, J.; Vos, B.; Foley, O.; Gleeson, D.; O'Gorman, E.; O'Keefe, R., Principles and applications of broadband acoustic resonance dissolution spectroscopy (BARDS): a sound approach for the analysis of compounds. Anal Chem 2012, 84 (5), 2202-10.
36. Fitzpatrick, D.; Scanlon, E.; Krüse, J.; Vos, B.; Evans-Hurson, R.; Fitzpatrick, E.; McSweeney, S., Blend uniformity analysis of pharmaceutical products by Broadband Acoustic Resonance Dissolution Spectroscopy (BARDS). International journal of pharmaceutics 2012, 438 (1-2), 134-139.
37. Ahmed, M. R.; McSweeney, S.; Krüse, J.; Vos, B.; Fitzpatrick, D., Contactless, probeless and non-titrimetric determination of acid–base reactions using broadband acoustic resonance dissolution spectroscopy (BARDS). Analyst 2018, 143 (4), 956-962.
38. Vos, B.; Crowley, S. V.; O'Sullivan, J.; Evans-Hurson, R.; McSweeney, S.; Krüse, J.; Ahmed, M. R.; Fitzpatrick, D.; O'Mahony, J. A., New insights into the mechanism of rehydration of milk protein concentrate powders determined by Broadband Acoustic Resonance Dissolution Spectroscopy (BARDS). Food Hydrocolloids 2016, 61, 933-945.
39. de Jonge, R.; Barendrecht, E.; Janssen, L.; van Stralen, S., Gas bubble behaviour and electrolyte resistance during water electrolysis. International Journal of Hydrogen Energy 1982, 7 (11), 883-894.

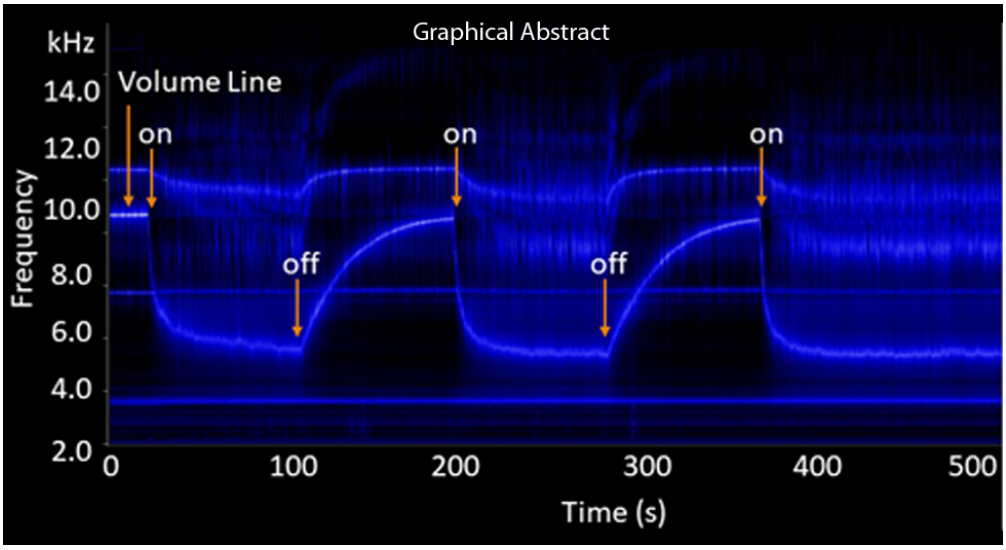
Graphical Abstract
kHz
Volume Line
14.0
12.0
10.0
8.0
6.0
4.0
2.0
Frequency
on
on
on
off
off
0
100
200
300
400
500
Time (s)